**Journal of Computing and Electronic Information Management**
ISSN: 2413-1660 | Vol. 21, No. 3, 2026

# Dynamic Reliability and Resilience Assessment of Jack-up Production Platform Legs Based on Dynamic Bayesian Networks

**Chao Zheng, Chuan Wang, Yunbo Zhang, Ze Feng**

School of Mechatronic Engineering, Southwest Petroleum University, Chengdu, China

**Abstract:** This paper proposes a dynamic reliability and system resilience assessment method for the leg structures of a mobile offshore production unit (MOPU) that is subjected to long-term service in complex marine environments. A fault tree of the leg system is first constructed and mapped to a Bayesian network (BN). Time slices are then introduced to expand the network into a dynamic Bayesian network (DBN). To capture history-dependent cumulative effects, a non-homogeneous state transition mechanism driven by physical damage laws is embedded within the DBN framework, within which the Melchers power-law corrosion model and the Palmgren-Miner fatigue model are dynamically modelled. A restoration sub-network comprising diagnosis capability, resource accessibility and maintenance capability is built, and a semi-Markov process is adopted to describe the transition probabilities of degradation and recovery. A quantitative resilience indicator is defined based on the "resilience triangle" theory. Numerical simulations are carried out for four typical scenarios: normal operation, frequent jacking operations, fishing-vessel collision, and blowout. The results show that fatigue degradation is the dominant factor affecting reliability; welded joints are the most sensitive nodes, and under collision/blowout conditions the sensitivity of stress-concentration nodes rises to the second highest; bottom-side collision combined with blowout.

**Keywords:** Mobile Offshore Production Unit (MOPU); Leg Structure; Dynamic Bayesian Network (DBN); Dynamic Reliability; System Resilience; Semi-Markov Process.

## 1. Introduction

The continuous growth of global energy demand and the cleaner utilisation of oil and gas resources under the "dual-carbon" goal are driving offshore oil and gas development towards deeper waters, marginal fields and regions with harsh climatic conditions. The mobile offshore production unit (MOPU) has become one of the key equipment for the cost-effective development of marginal fields because of its multi-functional integration of drilling, completion and early production, as well as its relatively low investment and flexible re-positioning and relocation capabilities [1]. As shown in Fig. 1, the MOPU relies on its legs standing on the seabed to support the topsides; the structural configuration makes the leg system the "lifeline" for the safe service of the platform.

Unlike conventional jack-up drilling rigs that move away after a single-well operation, the MOPU remains moored at the same well location for long-term continuous production, with a design service life typically up to 20-30 years [2]. During such a long service period, the leg structure continuously suffers from stochastic environmental loads (wind, waves and currents), cyclic alternating stresses induced by equipment operation, and electrochemical corrosion in the marine medium. In typhoon-prone areas such as the South China Sea, the 100-year return-period wave height can exceed 15 m; the wave impacts and vortex-induced vibrations caused by extreme sea states significantly aggravate structural fatigue damage [3-4]. In high-latitude cold regions, drifting sea ice may induce local plastic deformation and fracture hazards[5]. In addition, chloride ingress in seawater progressively reduces the metal wall thickness, creating a complex damage field combining general corrosion and pitting [6]. The time-varying coupling and long-term accumulation of the above multiple loads lead to a non-linear degradation trend of leg performance, and the service risk exhibits significant dynamic evolution characteristics.

Considerable work has been carried out by both academic researchers and the engineering community on the safety of leg structures. In the field of structural strength, Ding et al. [7] performed multi-condition static strength and buckling stability analyses of MOPU legs using non-linear finite element methods; Li et al. [8] systematically studied the fabrication technology and welding deformation control strategy for the legs of the POD-6 jack-up platform. Regarding environmental load calculation, codes such as DNV-RP-C205 and API RP 2A-WSD provide standard procedures for wave, current and wind loads [9-10], forming the basis for engineering design. In structural reliability assessment, traditional fault tree analysis (FTA) and Bayesian networks (BN) have been successfully applied to failure mode identification and probabilistic risk quantification of leg systems [11-12]. Shao et al. [13] introduced system safety engineering theory into offshore structure assessment and emphasised the construction of multi-level logical relationships.

However, most of the above studies are based on deterministic design loads or static reliability assumptions, and three major deficiencies can be identified. First, although the standard Markov chain can describe state transitions, its exponential sojourn-time assumption cannot capture the seasonal fluctuation of corrosion rate, the randomness of repair duration after fatigue damage accumulation, and other engineering realities [14]. Second, the existing frameworks often treat structural degradation and maintenance separately, lacking a closed-loop dynamic tracking capability for the entire lifecycle of "damage initiation → performance degradation → failure occurrence → emergency response →

system recovery" [15]. Third, for sudden emergency scenarios such as mechanical wear and soil disturbance due to frequent jacking[16], local buckling and weld brittleness induced by ship collision [17], and high-temperature erosion and impact loads during blowout[18], very few studies have incorporated them into a unified dynamic reliability-resilience quantification system. In particular, system resilience – as a measure of the ability of an engineering structure to quickly restore itself to an acceptable performance level after a disturbance – still lacks a clear definition and quantitative calculation method in the MOPU leg domain.

To this end, this paper proposes a new comprehensive assessment method for dynamic reliability and resilience of MOPU leg structures based on dynamic Bayesian networks (DBN) and semi-Markov processes. The novelty lies in three aspects: (1) In degradation modelling, by expanding the BN topology into discrete time slices, a non-homogeneous transition mechanism driven by physical laws is established, within which the Melchers power-law corrosion model and the Palmgren-Miner fatigue model are embedded into the dynamic framework to precisely characterise the continuous degradation path over time. (2) In recovery modelling, for the first time, diagnosis capability (based on MTTD), resource accessibility (spare parts and transport) and maintenance capability (based on MTTR) are built as a restoration sub-network; the semi-Markov process is introduced to describe non-exponential transition probabilities during the recovery phase, overcoming the inherent limitation of the traditional exponential assumption [19]. (3) In the evaluation metric, the "resilience triangle" theory is combined to define the system resilience value Ψ, achieving a shift from a single failure probability to a three-dimensional assessment covering degradation rate, minimum performance, and recovery speed.

Based on the above model, numerical simulations are carried out for four typical engineering scenarios – normal continuous operation, frequent jacking, fishing-vessel collision, and blowout – to systematically analyse the time-varying sensitivity of key leg nodes, degradation curves, and resilience differences under each scenario. The findings provide theoretical support and computational tools for MOPU life-extension decisions, inspection-window optimisation, and emergency resource allocation.

**Figure 1:** Basic structure of the MOPU

## 2. Methodology

**(1) Fault tree analysis (FTA)**

Fault tree analysis is based on backward deductive reasoning. The analysis procedure is shown in Fig. 2, consisting of qualitative analysis (minimal cut sets) and quantitative analysis (probability propagation). A Bayesian network (BN) is composed of a directed acyclic graph (DAG) and conditional probability tables (CPT). The mapping rules from FTA to BN are given in Table 1, and the detailed mapping process is illustrated in Fig. 3. By introducing time slices to expand the static BN, a dynamic Bayesian network (DBN) is formed. To account for degradation accumulation and structural memory, the state transitions between adjacent slices are parameterized as non-homogeneous functions driven by continuous physical damage variables, which can describe the dynamic evolution of system performance over time.

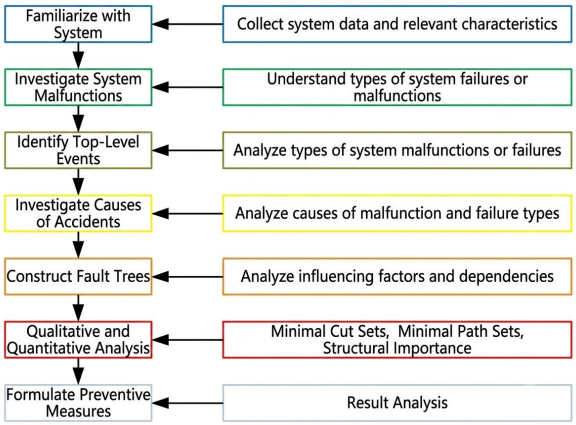


**Figure 2.** FTA analysis flow

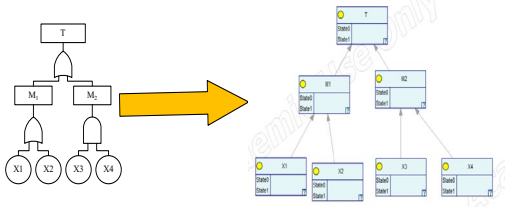

**Figure 3.** Mapping process from fault tree to BN

**Table 1.** Mapping relationship between fault tree and Bayesian network.)

| | |
|---|---|
| Basic event | Root node |
| Intermediate event | Intermediate node |
| Top event | Leaf node |
| Logic gate | Conditional probability table |
| Probability of basic event | Prior probability of root node |

**(2) Markov and semi-Markov processes**

In a DBN, the evolution of system performance is essentially the cumulative result of state transitions of each node across discrete time slices. A standard discrete-time Markov chain assumes that the state transition probability matrix is constant over time (homogeneous) and that the sojourn times follow a memoryless exponential distribution. However, the actual degradation process of leg structures exhibits significant non-homogeneity: the corrosion rate fluctuates with seasonal sea conditions, the propagation rate of fatigue cracks accelerates exponentially after initiation, and repair times show heavy-tailed characteristics due to spare-part logistics and personnel allocation. If a constant transition rate is adopted, the failure risk in the mid-to-late period will be severely underestimated.

Therefore, this paper introduces a semi-Markov process within the DBN framework to describe the state transitions of nodes. The core improvements are embodied in two aspects:

**1). Time-varying transition probabilities**

Let the system state at discrete time step $t$ be $S_t$ (taking values in a finite state space). The transition probability to state $S_{t+1}$ at time $t+1$ is no longer constant but a time-varying function driven by the accumulated physical damage at the current time. Specifically, the element $P_{ij}(t)$ of the transition probability matrix $\mathbf{P}(t)$ is expressed as:

$$P_{ij}(t) = \Pr\{S_{t+1} = j \mid S_t = i, \Theta(t)\}$$

where $\Theta(t)$ is the real-time damage feature vector at time $t$, including the corrosion depth $d(t)$ calculated by the Melchers model, the fatigue damage $D(t)$ computed by the Palmgren-Miner linear damage accumulation rule, and the comprehensive recovery rate $C(t)$ output from the restoration sub-network. This setting breaks the constraint of exponential sojourn times and allows the degradation and recovery rates to adaptively adjust with the service process, matching engineering realities such as seasonal corrosion fluctuations and accelerated crack propagation.

**2). Degradation-recovery decoupled transition**

Considering that the rise and fall of leg performance originate from two essentially different driving forces – physical degradation and manual intervention – this paper decomposes the state transition matrix into a degradation transition sub-matrix $\mathrm{P}_d(t)$ and a recovery transition sub-matrix $\mathrm{P}_r(t)$ via a weighted composition:

$$\mathbf{P}(t) = \mathbf{P}_d(t) \cdot (1 - \eta(t)) + \mathbf{P}_r(t) \cdot \eta(t)$$

where $\eta(t)$ is a binary variable (0 or 1) indicating whether maintenance intervention occurs at the current time step (determined by the diagnostic trigger condition of the restoration sub-network). This decoupling ensures that, in the absence of maintenance, performance strictly follows a monotonic degradation law; when maintenance is introduced, the recovery path based on the semi-Markov sojourn-time distribution is invoked, thereby accurately capturing the non-stationary process of "sudden failure → rapid response → gradual recovery".

Based on the above semi-Markov framework, Section 3 will provide the physical calculation models for corrosion depth $d(t)$ and fatigue cumulative damage $D(t)$, and on this basis, establish mapping rules from continuous physical damage quantities to discrete state levels (e.g., corrosion grades I–IV and fatigue damage threshold intervals), ultimately forming a step-by-step dynamic update strategy for the conditional probability tables (CPT) of the DBN at each time slice.

# 3. Modelling of leg degradation and recovery

Following the semi-Markov state-transition mechanism described in Section 2(2), this section constructs the physical degradation and functional recovery models of the leg structure. The bridge between the two lies in transforming the continuous damage evolution laws of corrosion and fatigue into updates of the prior failure rates of the root nodes (basic events) in the DBN at each discrete time step, thus providing quantitative basis for the time-varying assignment of $\mathbf{P}_d(t)$.

The mapping logic from physical degradation to DBN parameters is as follows.

## 3.1. Corrosion dimension

The corrosion depth $d(t)$ at any time $t$ is calculated by the Melchers power-law model:

$$d(t) = k \cdot t^n$$

According to the ratio of corrosion depth to wall thickness, it is mapped to grades I–IV as listed in Table 2. When the grade jumps, the failure rate of the "insufficient wall thickness" node in the fault tree is multiplied by a corresponding factor (for example, a 10% wall-thickness reduction multiplies the base failure rate $4.0 \times 10^{-6}$ by 1.5; a 30% reduction multiplies it by 5.0; the specific factors are determined by the API RP 2A residual-strength formula).

**Table 2.** Corrosion grades of the leg

| Corrosion grade | Corrosion depth / wall thickness ratio | Effect on residual strength |
|---|---|---|
| I | <10% | No obvious strength reduction; immediate repair not required |
| II | 10%~20% | Local stress increases; fatigue-sensitive zones need attention |
| III | 20%~50% | Compressive/bending capacity significantly reduced; risk exists |
| IV | >50% | Loss of structural integrity; possible sudden fracture |

## 3.2. Fatigue dimension

Based on the Palmgren-Miner linear cumulative damage rule and structural residual strength degradation theory, combined with the X-class S-N curve recommended by DNV-RP-C203, the fatigue damage is expressed as:

$$D(t) = \sum \frac{n_i}{N_i}$$

When $D(t)$ exceeds the preset thresholds of 0.1, 0.5 and 0.8, the failure rates of the "cyclic loading effect" and "stress concentration point" nodes are raised successively, reflecting the accelerated effects of fatigue crack initiation and propagation.

Wave load calculation adopts Airy wave theory (Figs. 4 and 5), and the wave force per unit leg length is computed by the Morison equation (including inertia and drag components). The stress amplitude and number of cycles are used as input nodes to establish the fatigue-degradation Bayesian network shown in Fig. 6.

## 3.3. Recovery dimension

The recovery capability of the leg system is composed of three sub-models:

(1) Diagnosis capability (D): evaluated through the restoration sub-network (as shown in Fig. 7). Instead of using an uncalibrated empirical algebraic equation, D is modeled as a target node whose conditional probability table (CPT) non-linearly aggregates the probabilistic states of its parent nodes, including Sensor Accuracy, Data Processing Efficiency, and Fault Response Time, reflecting the mean time to detect (MTTD) under uncertainty;

(2) Resource accessibility (R): considering spare-part stock rate, transport time (MTT transport) and personnel adequacy;

Maintenance capability (M): considering maintenance personnel skill, tool availability and repair duration (MTTR).

(3)The comprehensive recovery rate is obtained as $C = w_1 D + w_2 R + w_3 M$, where the weights are determined by the

analytic hierarchy process (AHP) based on scores from five offshore engineering experts, giving $w_1 = 0.35, w_2 = 0.40, w_3 = 0.25$ (consistency ratio $CR < 0.1$ ). The rate $C$ serves as the rate parameter of $\mathbf{P}_r(t)$ during maintenance time steps, determining the slope of performance rebound. The Bayesian network of the recovery model is shown in Fig. 7. Under the four scenarios (normal, frequent jacking, collision and blowout), and the comprehensive recovery rates are listed in Table 3.

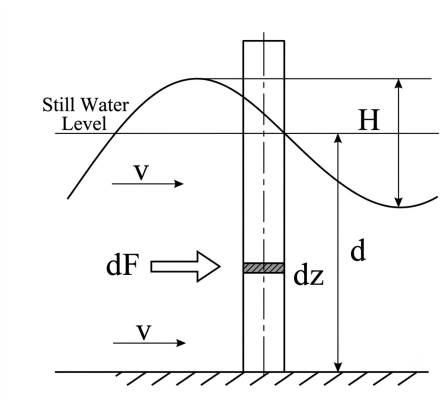


**Figure 4.** Wave composition

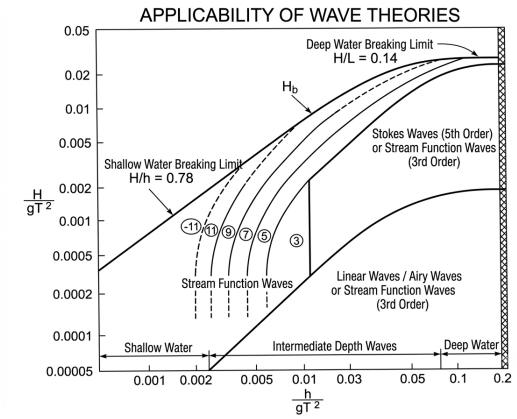


**Figure 5.** Basis for wave theory selection

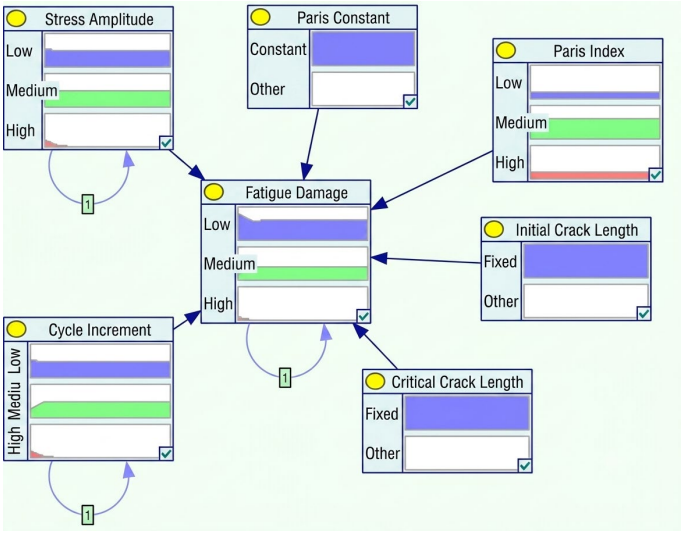


**Figure 6.** Fatigue degradation simulation model

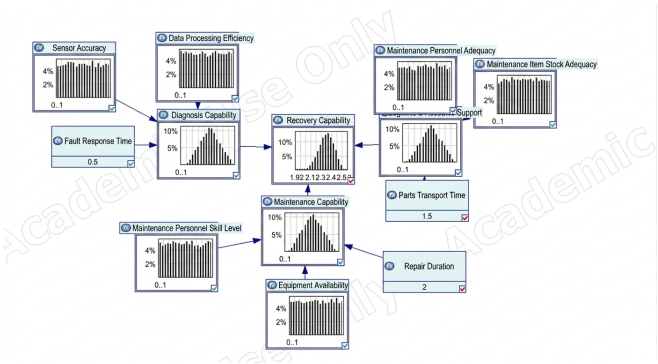


**Figure 7.** Bayesian network of the recovery model

**Table 3.** Comprehensive recovery rate calculation parameters

| Scenario | D | R | M | C |
|---|---|---|---|---|
| Normal | 0.98 | 0.95 | 0.90 | 0.943 |
| Jacking | 0.95 | 0.90 | 0.85 | 0.900 |
| Collision | 0.90 | 0.75 | 0.77 | 0.801 |
| Blowout | 0.90 | 0.40 | 0.67 | 0.631 |

## 3.4. Quantitative resilience indicator

Based on the "resilience triangle" and "bathtub curve" principles. The resilience value Ψ is taken as the ratio of the area under the degradation-recovery curve to the ideal rectangular area:

$$\Psi = \frac{\int_{t_0}^{t_4} P(t)\,dt}{P_0 \cdot (t_4 - t_0)}$$

# 4. Reliability analysis under different scenarios

## 4.1. Normal operation scenario

### 4.1.1. Platform parameters and fault tree

The main design parameters of the platform legs are given in Table 4, and the initial operating sea states in Table 5. The corresponding BN model under normal conditions in Fig. 8.

**Table 4.** Overall leg parameters of the MOPU

| Item | Value |
|---|---|
| Leg diameter | 3.5m |
| Leg length | 82m |
| Longitudinal leg spacing | 39.5m |
| Transverse leg spacing | 36m |
| Spudcan diameter | 7.4m |
| Spudcan height | 2.0m |

**Table 5.** Design operating parameters

| Item | Value |
|---|---|
| Water depth | 36m |
| Penetration depth | 12.6m |
| Design wind speed | 45.1m/s |
| Wave height | 14.3m |
| Wave period | 10.9s |
| Surface current velocity | 1.38m/s |
| Bottom current velocity | 0.81m/s |

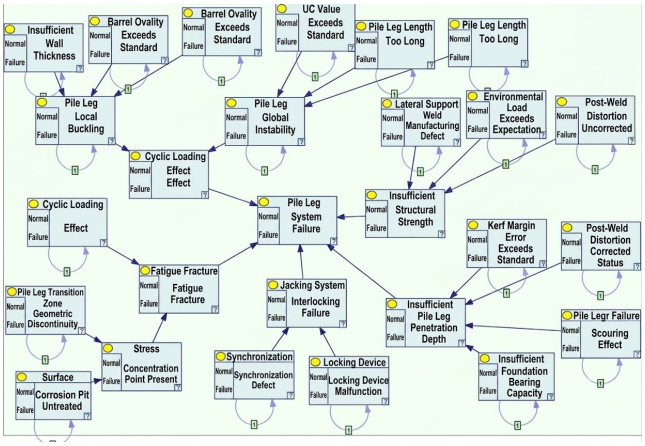


**Figure 8.** BN model under normal conditions

### 4.1.2. Results and discussion

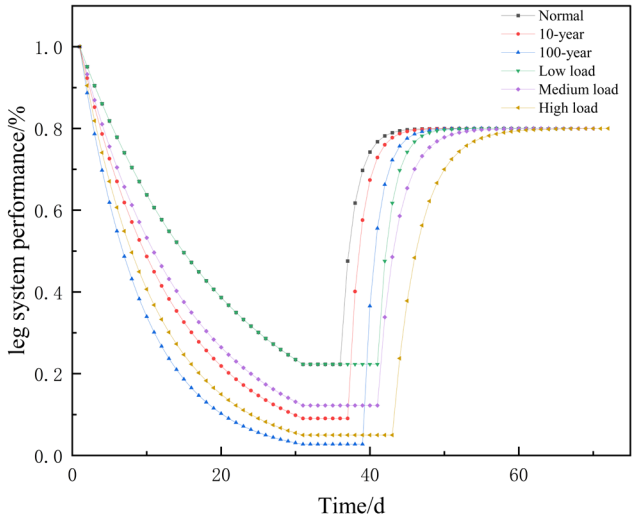


**Figure 9.** Degradation-recovery process

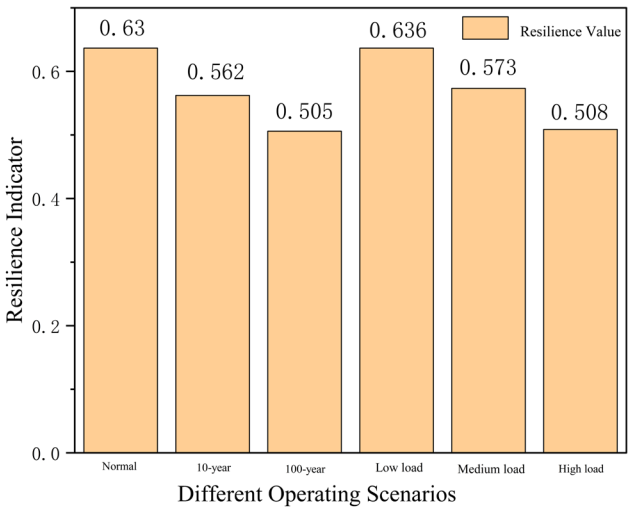


**Figure 10.** Resilience values under different working conditions

(1) Without human intervention, the macroscopic envelope curve of system reliability can be fitted by an exponential function $R(t) = Ce^{-\lambda t}$ ( $\lambda \approx 0.0518$ /step) with a goodness-of-fit $R^2 > 0.95$. This exponential expression is only a simplified mathematical characterisation of the final simulation curve shape; it does not represent the underlying transition probability assumption of the DBN, which strictly follows the semi-Markov time-varying rules defined in Section 2.2. The reason why the macroscopic reliability envelope exhibits an exponential-like decay pattern (characterized by a decelerating loss rate in the later stage) rather than an accelerating drop is attributed to the initial high failure sensitivity of the structural welded joints. Once these primary weak spots fail early in the timeline, the structural load paths are redistributed across the remaining redundant leg components, which temporarily stabilizes the system reliability degradation profile before final catastrophic collapse.

(2) Under the 10-year and 100-year return-period sea states, the degradation rate increases significantly. Under the 100-year condition, the system reliability drops to 0.31 within 10 time steps. This accelerated degradation stems from the quadratic amplification effect of wave height on the drag term $F_D = \frac{1}{2}\rho C_D D u \mid u \mid$ in the Morison equation: when the wave height increases from the design value of 14.3 m to the 100-year level, the water-particle velocity $u$ increases by more than 40%, leading to an approximately 1.8-fold increase in the fatigue damage per cycle $n_i/N_i$, and the cumulative damage curve shifts from near-linear to exponential-like growth. This result indicates that for MOPUs in typhoon-prone areas, the 100-year sea state should be used as the benchmark for determining maintenance intervals, rather than the design wave height alone.

(3) The introduction of maintenance can restore leg performance to 0.9, but under high loads the recovery time is prolonged; maintenance does not alter the physical degradation law, only postpones the degradation process – because repairs can only fix geometric defects and surface coatings, not the accumulated fatigue dislocation and microstructural deterioration caused by corrosion products, hence full recovery to the initial intact state (1.0) is impossible.

(4) The degradation-recovery curve shows that the performance can be restored to 80% within 30 steps, but cannot reach 100% due to irreversible damage. The resilience values under different working conditions are highest under

low loads (about 0.63) and decrease with increasing load; wave-current loads have a greater influence than operational loads.

## 4.2. Frequent jacking scenario

### 4.2.1. Damage mechanism and model adjustment

Frequent jacking (about 200 operations per year) causes mechanical wear, coating damage, accelerated electrochemical corrosion and soil disturbance (Fig. 11). Accordingly, the failure rates of fatigue- and corrosion-related nodes are increased by 20%, and that of the spudcan shear-failure node by 25%. The modified BN under frequent jacking is shown in Fig. 12.

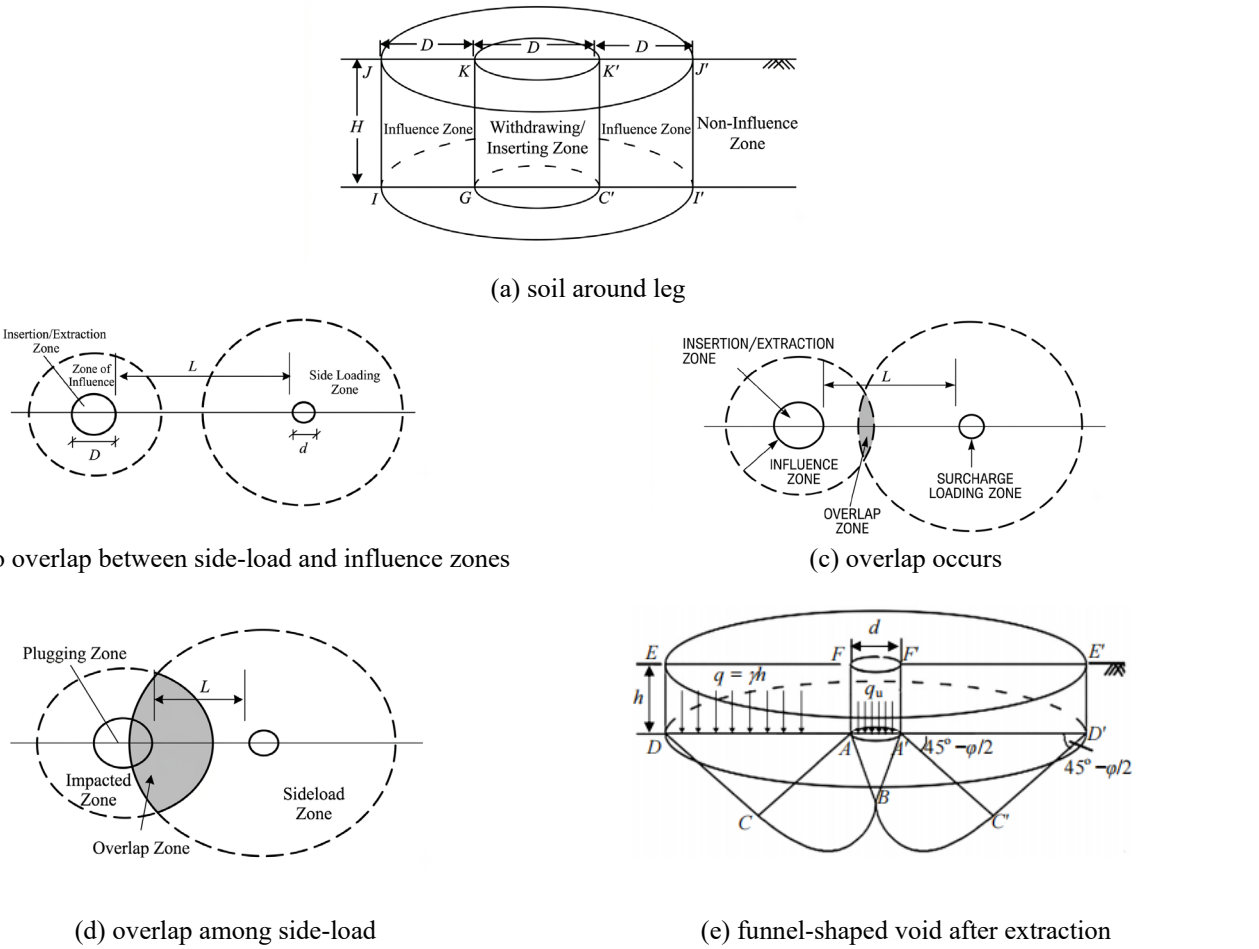


(a) soil around leg

(b) no overlap between side-load and influence zones

(c) overlap occurs

(d) overlap among side-load

(e) funnel-shaped void after extraction

**Figure 11.** Schematic of frequent jacking

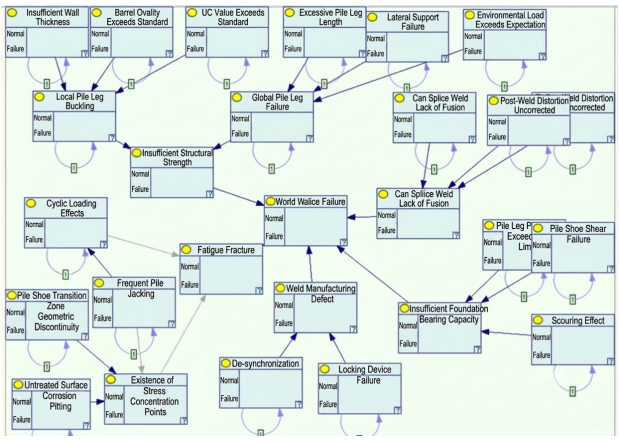


**Figure 12.** Schematic of frequent jacking

### 4.2.2. Results and discussion

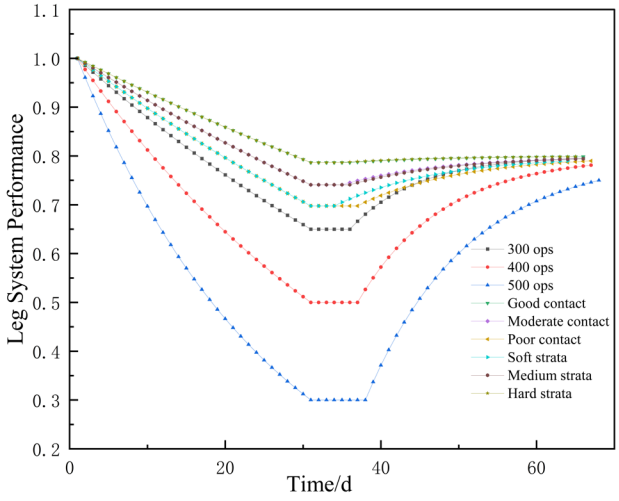


**Figure 13.** Degradation-recovery process

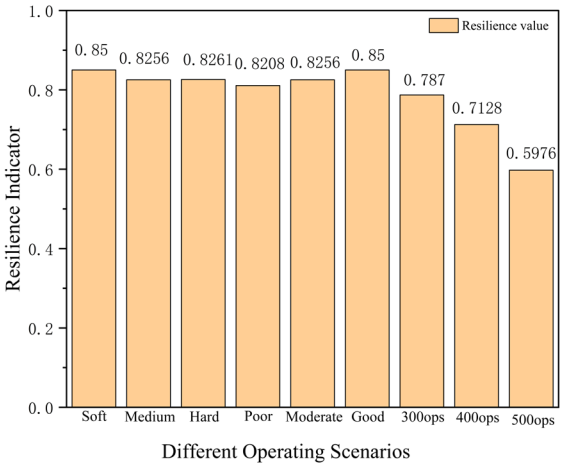


**Figure 14.** Resilience values under different conditions

(1) Contact condition effect: poorer contact leads to faster degradation. The performance curve exhibits a "slow-then-rapid" characteristic. It is recommended to initiate maintenance when performance falls below 80%.

(2) Strata type effect: soft strata show the fastest degradation, while hard strata show the slowest ; after 30 steps the maximum difference exceeds 0.06, indicating that strata conditions should be a key consideration in design.

(3) Jacking frequency effect: when the frequency increases from 300 to 500 times per year, the residual performance after 30 days drops from 0.70 to 0.30 , with a "fast-then-slow" degradation pattern.

(4) Recovery and resilience: as shown in Fig. 14(d), recovery is slower in soft strata, and high-frequency jacking aggravates cumulative damage. Resilience values are highest for good contact and hard strata (about 0.85), and decrease significantly at 500 operations/year.

## 4.3. Emergency scenarios

### 4.3.1. Collision damage mechanism

**Figure 15.** Squash-type buckling

The collision energy of a fishing vessel is estimated by the kinetic energy formula $E = \frac{1}{2}mv^2$ (vessel weight 1000 t, speed 0.5-2 m/s, energy 0.06-10 MJ). Collision causes plastic indentation of the tube wall, section thinning of 20-30%, reduction of local buckling critical load to 10% of the original value, and induces "squash-type" buckling (Fig. 15). Crack initiation in the weld heat-affected zone is accelerated, and shear failure zones appear in the foundation (Fig. 16). Nodes related to local buckling, global instability, insufficient penetration depth and scour effect are introduced. The BN for the collision scenario is shown in Fig. 17.

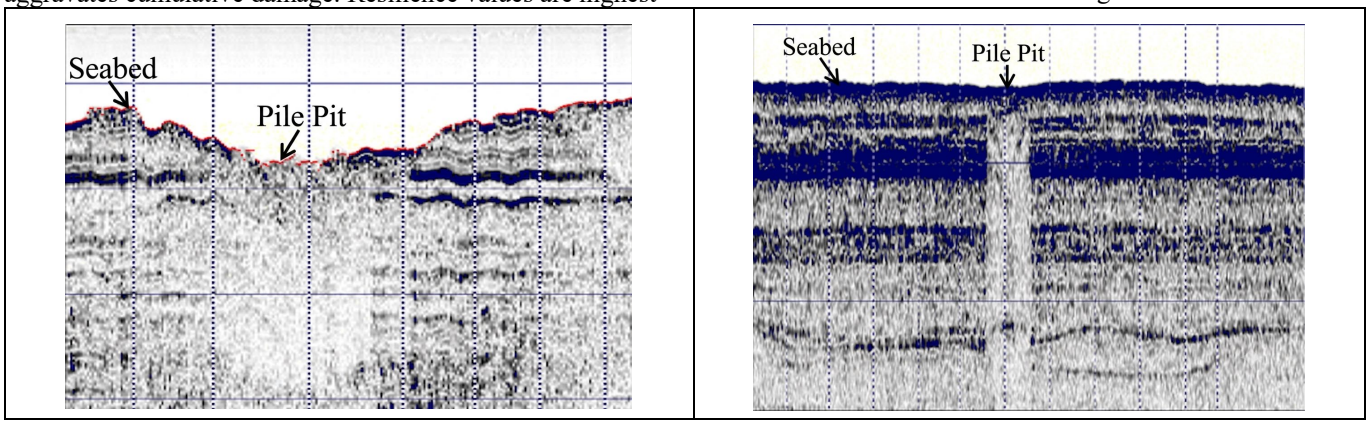


**Figure 16.** Shallow stratigraphic in the region

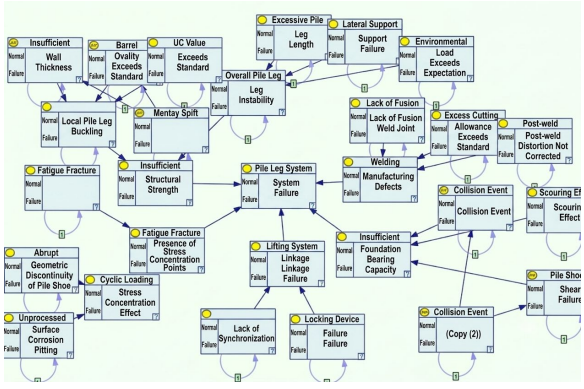


**Figure17.** BN for collision-induced degradation

### 4.3.2. Results and discussion

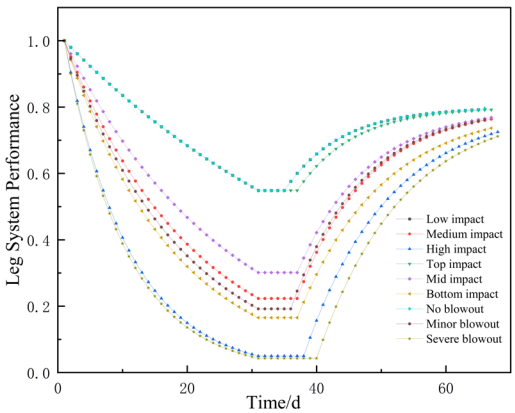


**Figure 18.** Degradation-recovery process

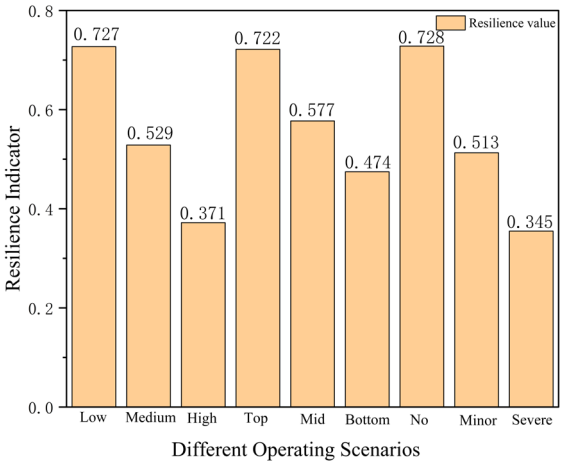


**Figure 19.** Resilience values under different conditions

(1) Impact intensity effect: under low-intensity impact, residual performance after 30 days remains >55%; under medium-to-high intensity, performance drops sharply to near-failure.

(2) Impact location effect: bottom-side collision causes the fastest degradation (only 20% remaining after 30 days), followed by mid-side and then top-side. The reason is that the bottom connection has more welds and the soil bearing capacity is more prone to loss.

(3) Blowout coupling: when collision triggers a blowout, performance rapidly falls to the failure threshold; both mild and severe blowouts lead to irreversible damage.

(4) Recovery and resilience: the degradation-recovery curve shows that high-damage cases require longer recovery times and initial rapid-recovery procedures are needed. Resilience values are lowest (about 0.30) under severe blowout conditions.

### 4.4. Comprehensive comparison and discussion

Welded joints exhibit the highest sensitivity among all nodes across all scenarios (their posterior probability increment $\Delta P$ ranges from 0.12 to 0.18). Under collision/blowout conditions, the $\Delta P$ of stress-concentration nodes rises from 0.07 under normal conditions to 0.15, ranking second – this is attributed to the local plastic dent caused by collision, which significantly increases the stress concentration factor (theoretically from 2.5 to 4.2) and shortens the crack-initiation life by about 60%.

The system resilience values for the four scenarios rank as: frequent jacking (up to 0.85) > normal operation (0.63) > collision (0.45-0.55) > collision + blowout (0.30). The resilience under frequent jacking surpasses that under normal operation because the degradation is periodic and maintenance windows are predictable, whereas the long-term irreversible cumulative damage under normal operation lacks periodic resetting opportunities. The blowout-coupled case has the lowest resilience, as high-temperature erosion accelerates corrosion kinetics (Arrhenius effect, rate multiplier about 2-3) and simultaneously reduces resource accessibility ($R$ drops to 0.40 in Table 3).

Based on the above comparison, the following recommendations are made:

(a) For frequently jacked platforms, priority should be given to strata investigation and contact-state maintenance, with a resilience target set above 0.80.

(b) For long-term moored platforms in typhoon areas, the 100-year sea state should be used as the maintenance trigger; planned maintenance should be initiated when reliability drops to 0.65.

(c) For high-collision-risk areas, bottom-structural fenders should be installed, and the emergency response time target should be set to $t_4 - t_2 \leq 5$ steps (approximately 15 days); otherwise the resilience will fall below the safety threshold of 0.35.

## 5. Conclusions and future work

### 5.1. Conclusions

(1) A dynamic reliability assessment model for leg structures, combining fault-tree analysis and DBN with semi-Markov time-varying transition mechanisms, has been established, enabling quantitative analysis of the entire degradation-recovery process.

(2) Fatigue degradation is the dominant factor in leg performance attenuation. Welded joints have the highest sensitivity, with a posterior probability increment of 0.12-0.18; under collision/blowout conditions, the increment for stress-concentration nodes rises from 0.07 to 0.15, ranking second.

(3) In frequent-jacking scenarios, soft strata and high-frequency operations significantly accelerate degradation, with a clear reduction in resilience values.

(4) The bottom-side collision combined with blowout case is the most hazardous, with a resilience value of only 0.30 – 52% lower than the normal condition – and the required recovery time is extended to more than 20 steps.

### 5.2. Future work

(1) Introduce a three-stage degradation model (early failure, stable period, wear-out period) to replace the pure exponential model.

(2) Integrate SHM monitoring data (strain, acoustic emission, etc.) and combine with digital twin and deep learning to achieve adaptive model calibration.

(3) Use online monitoring data to dynamically update DBN parameters, thereby improving fault-diagnosis accuracy and resource-allocation efficiency.

## References

[1] China made the world's first self-elevating natural gas compression platform. (2015). Cryogenic Technology, (7), 36.

[2] Wu, S. B., & Wang, C. L. (2020). Strength calculation and analysis of jack-up platform legs in storm self-preservation state. Ship Standardization Engineer, 53(6), 48-52.

[3] Jiang, Y. M., Yu, D. H., Li, G., Zhang, Y. S., & Song, J. W. (2025). Extreme environment condition model of wind-wave-swell and its associated structural analysis. Acta Oceanologica Sinica, 47(12), 70-83.

[4] Jia, X., Jia, L. S., Huang, J., Li, H. W., & Wang, X. T. (2021). Overall scheme study of steel catenary riser for "Deep Sea No. 1" energy station. China Offshore Oil and Gas, 33(5), 165-174.

[5] Liu, L., Yin, Z. Y., & Ji, S. Y. (2019). A high-performance dilated polyhedral discrete element method for ice loads on ships and offshore platform structures. Chinese Journal of Theoretical and Applied Mechanics, 51(6), 1720-1739.

[6] Liu, Y. M., Yang, L., Rao, F., & Wang, H. B. (2023). Research progress on chloride-induced corrosion of steel reinforcement in marine concrete. Bulletin of the Chinese Ceramic Society, 42(9), 3059-3074.

[7] Ding, Y. (2009). Structural strength analysis of jack-up platform legs [Master's thesis]. Shanghai Jiao Tong University.

[8] Li, Q. (2016). Research on leg construction technology of POD-6 jack-up drilling platform. Offshore Engineering Equipment and Technology, 3(3), 159-162.

[9] Det Norske Veritas. (2014). DNV-RP-C205: Environmental conditions and environmental loads (DNV Recommended Practice). DNV.

[10] API RP 2A-WSD. (2014). Recommended practice for planning, designing and constructing fixed offshore platforms (API Recommended Practice 2A-WSD). American Petroleum Institute.

[11] Li, Z., Hu, S. P., Gao, G. P., & Liu, C. (2020). Bayesian decision model for berthing risk under different tidal current conditions. Journal of Shanghai Maritime University, 41(1), 57-63.

[12] Dai, Q. L., Li, H. E., Wu, S. H., & Chen, Y. F. (2024). Cost assessment of submarine cable route towing based on Bayesian network. China Sciencepaper, 19(10), 1142-1150.

[13] Shao, H. (2008). System safety engineering. Petroleum Industry Press.

[14] Zhang, J. L., Zhang, J. X., Du, D. B., & Wu, Y. H. (2025). Remaining useful life prediction for equipment with multiple degradation features considering time-varying dependence. Journal of Xi'an Jiaotong University, 59(10), 210-220.

[15] Wang, H. P., & Chen, D. Y. (2023). Research and application of structural health monitoring technology for offshore jacket platforms. Petroleum and Natural Gas Chemical Industry, 52(2), 157-164.

[16] Liu, R., Cao, T. M., Chen, G. S., & Zhang, L. (2020). Study on the influence of spudcan jacking and extraction on the bearing capacity of adjacent spudcans. Rock and Soil Mechanics, 41(9), 2943-2952.

[17] Zhang, A. F., Liu, S. K., Yao, M. M., & Wang, Z. (2021). Analysis of structural damage and ship impact force in ship-bridge collision. Journal of Chongqing Jiaotong University (Natural Science Edition), 40(3), 121-127.

[18] Liu, J. H. (2025). Fault tree analysis of single-well dual-bore blowout based on FTA method. China Petroleum and Chemical Standards and Quality, 45(9), 4-6.

[19] Bobbio, A., Portinale, L., Minichino, M., & Ciancamerla, E. (2001). Improving the analysis of fault trees with imprecise probabilities. Reliability Engineering & System Safety, 71(2), 149-166. https://doi.org/10.1016/S0951-8320(00)00088-5